Spinor Bose-Einstein condensates of rotating polar molecules

Y. Deng[1] and S. Yi[1,2]

[1]*State Key Laboratory of Theoretical Physics, Institute of Theoretical Physics, Chinese Academy of Sciences, P.O. Box 2735, Beijing 100190, China*

[2]*Synergetic Innovation Center for Quantum Effects and Applications, Hunan Normal University, Changsha 410081, China*

(Received 1 December 2014; revised manuscript received 14 April 2015; published 25 September 2015)

We propose a scheme to realize a pseudospin-1/2 model of the $^1\Sigma(v=0)$ bialkali polar molecules with the spin states corresponding to two sublevels of the first excited rotational level. We show that the effective dipole-dipole interaction between two spin-1/2 molecules couples the rotational and orbital angular momenta and is highly tunable via a microwave field. We also investigate the ground-state properties of a spin-1/2 molecular condensate. A variety of nontrivial quantum phases, including the doubly quantized vortex states, are discovered. Our scheme can also be used to create spin-1 model of polar molecules. Thus we show that the ultracold gases of bialkali polar molecules provide a unique platform for studying the spinor condensates of rotating molecules.

DOI: 10.1103/PhysRevA.92.033624 PACS number(s): 03.75.Mn, 03.75.Nt, 67.85.−d, 73.43.Cd

I. INTRODUCTION

Recent experimental realizations of ultracold polar molecules in rovibrational ground state [1–6] offer remarkable new frontiers for many areas of science, such as precision measurement [7–9], quantum information [10], quantum computation [11], ultracold collisions [12,13], cold controlled chemistry [14,15], and quantum simulation [16–18]. Particularly, from the condensed-matter perspective, the large permanent electric dipole moment and the ability to control the hyperfine states within a single rovibrational level [19,20] make ultracold polar molecules an ideal platform for investigating strongly correlated many-body physics [21–23]. So far, the dipolar spin-exchange interactions [24] and the many-body dynamics [25] have been experimentally observed in lattice-confined ultracold KRb gases.

For rotating molecules, the net dipole moment in the laboratory frame vanishes in the absence of a dc electric field. Hence in most theoretical many-body studies, a strong dc electric field is assumed to align polar molecules. Consequently, the rotational degrees of freedom is frozen. Even though there exist multicomponent models by utilizing different rotational states, the number of molecules in each rotational state is independently conserved by the interactions. On the contrary, the spin-exchange contact interaction in atomic spinor Bose-Einstein condensates (BECs) results in rich magnetic phenomena [26–28]. Of particular interest, the magnetic dipole-dipole interaction (DDI) gives rise to spontaneous spin textures in dipolar spinor BECs [29–32].

In this paper we show that a bialkali polar molecule in the electronic and vibrational ground state can be modeled as a pseudospin-1/2 molecule with the spin states corresponding to two hyperfine sublevels of the first excited rotational level. The effective DDI between molecules contains a rotation-orbit coupling term that is capable of inducing spin mixing. Thus a BEC formed by these spin-1/2 molecules represents a spinor BEC instead of a two-component BEC. We also study the ground-state phases of the spin-1/2 molecular BEC and demonstrate that rotation-orbit-coupled DDI gives rise to the doubly quantized vortex (DQV) phases. Although BECs of polar molecules are studied in Refs. [33–35], the DDI considered in these works does not contain a term that exchanges spin and orbital angular momentum.

This paper is organized as follows. In Sec. II, we introduce the model Hamiltonian for a pseudospin-1/2 molecule. Section III is devoted to derive the effective DDI between two pseudospin-1/2 molecules. In Sec. IV, we present the quantum phases of molecular condensates. In Sec. V, we briefly discuss the experimental feasibility of our model. Finally, we conclude in Sec. VI.

II. EFFECTIVE SINGLE-MOLECULE HAMILTONIAN

To be specific, we consider a gas of ^{7}Li ^{133}Cs molecules in $^1\Sigma(v=0)$ state subjected to a bias magnetic field $\mathbf{B}=B\hat{\mathbf{z}}$. Each molecule has three angular momentum degrees of freedom: the rotation angular momentum $\mathbf{N}$ and the nuclear spins $\mathbf{I}_1$ and $\mathbf{I}_2$ [36–38]. Its internal states can be characterized in the uncoupled basis $|M_1M_2NM_N\rangle$, where M_N and M_i are, respectively, the projections of $\mathbf{N}$ and $\mathbf{I}_i$ along the quantization z axis. The Hamiltonian describing the internal degrees of freedom includes rotational $\hat{H}_{\rm rot}$, hyperfine $\hat{H}_{\rm hf}$, and Zeeman $\hat{H}_Z$ terms. Among them, the rotational term, $\hat{H}_{\rm rot}=B_v\mathbf{N}^2$, defines the largest intrinsic energy scale as the rotational constant B_v is of gigahertz order. Since the rotational spectrum, $B_vN(N+1)$, is anharmonic, we may focus on the lowest two rotational levels with $N=0$ and 1, which are split by an energy $2B_v$.

Although the nuclear hyperfine interaction $\hat{H}_{\rm hf}$ mixes different internal states, it can be overcome by the Zeeman term $\hat{H}_Z$, which couples $\mathbf{B}$ to $\mathbf{N}$ and $\mathbf{I}_i$. For sufficiently strong magnetic field, the nuclear Zeeman effect dominates over the hyperfine interaction such that M_1 and M_2 become good quantum numbers. For LiCs, this magnetic field is around 40 G [39]. Focusing on the lowest nuclear Zeeman levels ($M_i=I_i$) in the $N=0$ and 1 manifolds, the relevant internal states reduce to $|N,M_N\rangle=|0,0\rangle$, $|1,0\rangle$, and $|1,\pm1\rangle$, which simplifies a rotating molecule to a four-level system (see Appendix A for details). It can be verified that the hyperfine interaction is diagonal in this reduced four-level Hilbert space. Therefore each of these four levels indeed possesses a definite quantum number M_N. In Fig. 1(a), we plot the magnetic field dependence of the hyperfine splittings $\delta_{0,-1}=E_{|1,0\rangle}-E_{|1,-1\rangle}$ and $\delta_{1,-1}=E_{|1,1\rangle}-E_{|1,-1\rangle}$ for a LiCs molecule. As can be seen, the typical hyperfine splitting is around a few tens of kilohertz for a magnetic field in the range of 100–900 G,

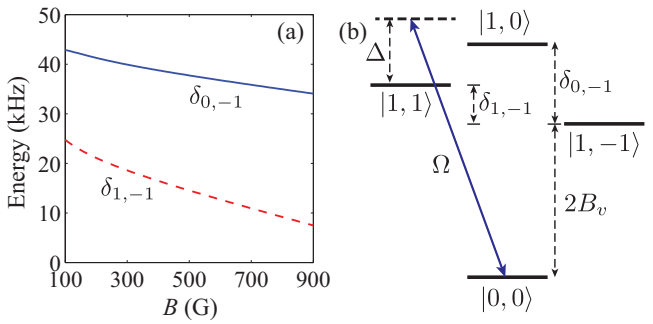

FIG. 1. (Color online) (a) Hyperfine splittings as functions of the external magnetic field and (b) level structure.

which corresponds to a temperature around 2 μ K. Figure 1(b) shows the corresponding level structure.

Next, we illuminate the molecules with a position-independent σ^+-polarized microwave field which couples to the electric dipole moment of the molecule $d\hat{\mathbf{d}}$, where d is the permanent electric dipole moment and $\hat{\mathbf{d}}$ is the unit vector along the internuclear axis of the molecule. The frequency of the microwave $\omega_{\rm mw}$ is assumed to be blue detuned relative to the rotational splitting with a detuning $\Delta = 2B_v/\hbar - \omega_{\rm mw}$, where the typical value of Δ is 100 MHz. The $|0,0\rangle \leftrightarrow |1,1\rangle$ transition is then induced by the microwave with Rabi frequency Ω. Assuming that all molecules are initially prepared in the $|1,1\rangle$ state [19], level $|0,0\rangle$ can be adiabatically eliminated in the large detuning limit $|\Omega/\Delta| \ll 1$. This procedure yields an effective level splitting $\delta = \delta_{1,-1} + \Omega^2/\Delta$ between the levels $|1,1\rangle$ and $|1,-1\rangle$. Moreover, under the condition $|\delta| \ll |\delta_{0,-1}|$, level $|1,0\rangle$ becomes well separated from $|1,\pm1\rangle$, which eventually leads to the effective pseudospin-1/2 single-particle Hamiltonian in the rotating frame (see the Appendix B):

$$\hat{h} = \frac{\mathbf{p}^2}{2m}\hat{I} + \hbar\frac{\delta}{2}\hat{\sigma}_z, \tag{1}$$

where m is the mass of the molecule, $\hat{I}$ is the identity matrix, and for shorthand notation, we shall denote $|1,1\rangle$ and $|1,-1\rangle$ as $|\uparrow\rangle$ and $|\downarrow\rangle$, respectively. As analyzed below, $|\uparrow\rangle$ and $|\downarrow\rangle$ form a closed Hilbert space even in the presence of the molecule-molecule interactions. On a side note, when $\delta_{1,-1} \sim 0$ under an appropriate magnetic field, we may also realize a spin-1 model by coupling $|0,0\rangle$ and $|1,0\rangle$ states with a large detuned π-polarized microwave field.

In the second-quantized form, the single-particle Hamiltonian for the spin-1/2 molecules takes the form

$$\hat{\mathcal{H}}_0 = \sum_\sigma \int d\mathbf{r}\hat{\psi}^\dagger_\sigma(\mathbf{r})[\hat{h}_{\sigma\sigma} + U_{\rm opt}(\mathbf{r})]\hat{\psi}_\sigma(\mathbf{r}), \tag{2}$$

where $\hat{\psi}_{\sigma=\uparrow,\downarrow}$ is the field operator for the spin-σ molecule and $U_{\rm opt}$ is the optical dipole trap, which is assumed to be spin independent [20,24].

III. INTERACTIONS

The electric DDI between two molecules, $d\hat{\mathbf{d}}_1$ and $d\hat{\mathbf{d}}_2$, can be expressed as

$$V_{\rm dd}(\mathbf{R}) = \frac{g_d}{|\mathbf{R}|^3}[\hat{\mathbf{d}}_1\cdot\hat{\mathbf{d}}_2 - 3(\hat{\mathbf{d}}_1\cdot\hat{\mathbf{R}})(\hat{\mathbf{d}}_2\cdot\hat{\mathbf{R}})], \tag{3}$$

where $g_d = d^2/(4\pi\epsilon_0)$ is the DDI strength, with ϵ_0 being the electric permittivity of vacuum, $\mathbf{R}$ is the vector connecting the molecules, and $\hat{\mathbf{R}} = \mathbf{R}/|\mathbf{R}|$. For a typical density $n = 10^{13}$ cm^{-3} of LiCs gas, the DDI energy $g_d n$ is around 46 kHz, which justifies the elimination of the $|0,0\rangle$ level. Although there is no direct DDI between states in the $N = 1$ manifold, effective DDI can be induced via the eliminated $|0,0\rangle$ state. As shown in Appendix C, in the rotating frame, the effective DDI that is time averaged over a period of $2\pi/\omega_{\rm mw}$ is

$$\begin{aligned}
\hat{\mathcal{H}}_{\rm dd} &= \hat{V}_1 + \hat{V}_2 + \hat{V}_3,\\
\hat{V}_1 &= \kappa g_d\sqrt{\frac{4\pi}{45}}\int\frac{d\mathbf{r}_1 d\mathbf{r}_2}{|\mathbf{R}|^3}Y_{20}(\hat{\mathbf{R}}) :\hat{n}_\uparrow(\mathbf{r}_1)\hat{n}_\uparrow(\mathbf{r}_2):,\\
\hat{V}_2 &= \kappa g_d\sqrt{\frac{4\pi}{45}}\int\frac{d\mathbf{r}_1 d\mathbf{r}_2}{|\mathbf{R}|^3}Y_{20}(\hat{\mathbf{R}}) :\hat{S}_+(\mathbf{r}_1)\hat{S}_-(\mathbf{r}_2):,\\
\hat{V}_3 &= \kappa g_d\sqrt{\frac{8\pi}{15}}\int\frac{d\mathbf{r}_1 d\mathbf{r}_2}{|\mathbf{R}|^3}[Y_{22}(\hat{\mathbf{R}}) :\hat{n}_\uparrow(\mathbf{r}_1)\hat{S}_-(\mathbf{r}_2): + \text{H.c.}],
\end{aligned} \tag{4}$$

where $\kappa = \Omega^2/\Delta^2$, Y_{lm} are spherical harmonics, and $\hat{n}_\sigma = \hat{\psi}^\dagger_\sigma\hat{\psi}_\sigma$, $\hat{S}_- = \hat{\psi}^\dagger_\downarrow\hat{\psi}_\uparrow$, $\hat{S}_+ = \hat{S}^\dagger_-$, and $:\hat{O}:$ arrange the operator in normal order. Clearly, $\hat{V}_1$ represents the density-density DDI between spin-$\uparrow$ molecules and $\hat{V}_2$ is the dipolar spin-exchange interaction between spin-$\uparrow$ and -$\downarrow$ molecules. Of particular interest, the dipolar density-spin interaction $\hat{V}_3$ couples the rotational and orbital angular momenta while keeping the total angular momentum conserved.

Compared to the DDI appearing in other spin-1/2 models of polar molecules [23,24,33], selecting $|1,1\rangle$ and $|1,-1\rangle$ states gives rise to the rotation-orbit coupling term $\hat{V}_3$. In addition, the elimination of the $|0,0\rangle$ state with a large detuned microwave field introduces a control knob κ for the DDI. Throughout this work, we assume that $\kappa \leqslant 6\times10^{-4}$ to maintain a stable BEC. Consequently, the typical DDI energy between states in the $N = 1$ manifold is around $\kappa g_d n \lesssim 27$ Hz, which further validates the assumption that $|1,0\rangle$ is well separated from $|1,\pm1\rangle$.

For completeness, we also include the collisional interaction term

$$\hat{\mathcal{H}}_{\rm con} = \sum_{\sigma\sigma'}\frac{2\pi\hbar^2 a_{\sigma\sigma'}}{m}\int d\mathbf{r}\hat{\psi}^\dagger_\sigma(\mathbf{r})\hat{\psi}^\dagger_{\sigma'}(\mathbf{r})\hat{\psi}_{\sigma'}(\mathbf{r})\hat{\psi}_\sigma(\mathbf{r}), \tag{5}$$

where $a_{\sigma\sigma'}$ are the s-wave scattering lengths between the spin-σ and -σ' molecules. So far, the s-wave scattering lengths for LiCs molecules are unknown. For simplicity, we take the typical values of $a_{\uparrow\uparrow} = a_{\downarrow\downarrow} = a_{\uparrow\downarrow} = 100a_B$, with a_B being the Bohr radius. It can be estimated that the contact interaction energy is also of a few tens of Hertz. We remark that the spin structures presented below should not depend on the specific choice of $a_{\sigma\sigma'}$, as $\hat{\mathcal{H}}_{\rm con}$ conserves the number of molecules in the individual spin states.

IV. RESULTS

We now turn to explore the ground-state properties of a molecular BEC by using the mean-field theory. To this end, we replace the field operators $\hat{\psi}_\sigma$ by the condensate wave functions $\psi_\sigma \equiv \langle\hat{\psi}_\sigma\rangle$, which can be obtained by numerically

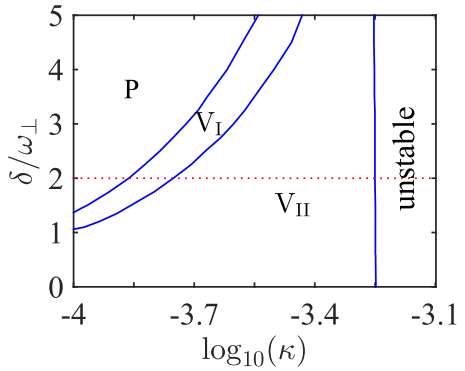

FIG. 2. (Color online) Phase diagram on the κ-δ parameter plane. The dotted line is a guide for the eyes.

minimizing the energy functional $\mathcal{F}[\psi_\sigma,\psi_\sigma^*] = \langle \hat{\mathcal{H}}_0 + \hat{\mathcal{H}}_{\rm dd} + \hat{\mathcal{H}}_{\rm con}\rangle$. More specifically, we consider a condensate of $\mathcal{N} = 3.2\times10^5$ LiCs molecules trapped in a harmonic potential $U_{\rm opt} = m\omega_\perp^2(x^2+y^2+\gamma^2z^2)/2$, with $\omega_\perp = (2\pi)10$Hz being the radial trap frequency and $\gamma = 6.3$ being the trap aspect ratio. For simplicity, the condensate wave functions are decomposed into $\psi_\sigma(\mathbf{r}) = \phi_\sigma(x,y)\phi_z(z)$ with $\phi_z(z) = (\gamma/\pi\ell_\perp^2)^{1/4}e^{-\gamma z^2/2\ell_\perp^2}$ and $\ell_\perp = \sqrt{\hbar/(m\omega_\perp)}$. After integrating out the z variable, the system simplifies to a quasi-two-dimensional system. Limited by the validity of the spin-1/2 model and the stability of the system, the numerical results presented below cover the parameter space $-10 \leqslant \delta/\omega_\perp < 10$ and $10^{-4} \leqslant \kappa \leqslant 6\times10^{-4}$.

Figure 2 summarizes the phase diagram of a molecular BEC in the κ-δ parameter plane. The region denoted by P represents the polarized phase and those labeled by V_I and V_{II} are two vortex phases. For $\kappa > 5.7\times10^{-4}$, the condensate becomes unstable due to the partially attractive nature of the DDI. In Figs. 3(a) and 3(b), we plot, for a fixed effective detuning $\delta = 2\omega_\perp$, the κ dependence of the numbers of molecules

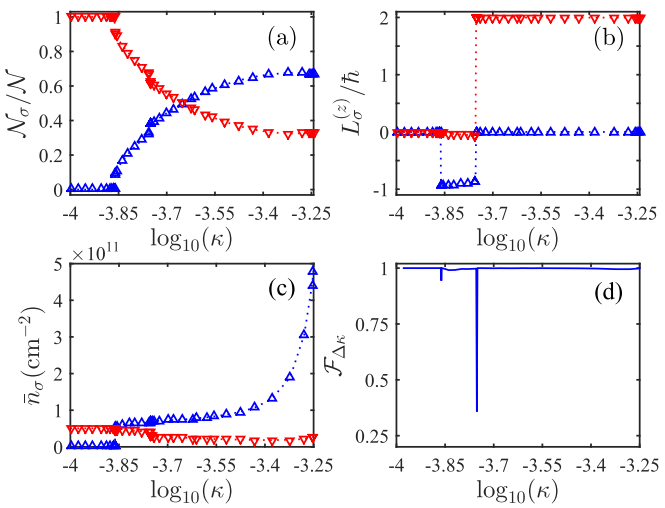

FIG. 3. (Color online) (a)–(c) The molecule number, mean orbital angular momentum, and peak density, respectively, as functions of κ for spin-↑ (△) and -↓ (▽) states. (d) Fidelity $\mathcal{F}_{\Delta\kappa}$ as a function of κ. The detuning used here is $\delta = 2\omega_\perp$.

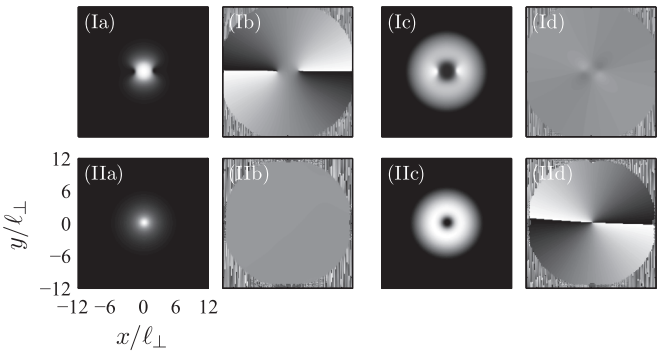

FIG. 4. Typical condensate wave functions for the vortex phases V_I (row 1) and V_{II} (row 2) corresponding to $\kappa = 1.56\times10^{-4}$ and 4.94×10^{-4}, respectively. The effective detuning used here is $\delta = 2\omega_\perp$. Columns 1 and 3 show the densities of the spin-↑ and -↓ molecules, respectively; columns 2 and 4 show the corresponding phases.

$\mathcal{N}_\sigma = \int dxdy|\phi_\sigma|^2$ and the average orbital angular momenta $L_\sigma^{(z)} = -i\hbar\mathcal{N}_\sigma^{-1}\int dxdy\phi_\sigma^*(x\partial_y - y\partial_x)\phi_\sigma$, respectively. In the P phase, the spin-↓ state is dominantly populated and the wave functions of both spin states are structureless; while in the vortex phases, molecules in one of the spin states carry orbital angular momentum. The boundaries between different phases are clearly marked by the $L_\sigma^{(z)}$. It should be noted that for large negative δ, we still find that $L_\downarrow^{(z)} = 2\hbar$, even though only the spin-↑ state is dominantly populated. Figure 3(c) shows the κ dependence of the peak number densities $\bar{n}_\sigma = \max(n_\sigma)$ with $n_\sigma = |\phi_\sigma|^2$. It should be noted that $\bar{n}_\uparrow > \bar{n}_\downarrow$ immediately after the spin-↑ state is populated. To further confirm these phase transitions, we calculate the fidelity, $\mathcal{F}_{\Delta\kappa} = |\langle\Psi(\kappa)|\Psi(\kappa+\Delta\kappa)\rangle|$, of the condensate wave function $|\Psi\rangle = (\psi_\uparrow,\psi_\downarrow)^T$, where $\Delta\kappa$ is the interval of κ between two adjacent data points [40]. Since the fidelity measures the similarity between two adjacent states in the parameter space, it can drop sharply across different phases [41,42]. In Fig. 3(d) we plot the κ dependence of $\mathcal{F}_{\Delta\kappa}$. Two transition points marked by the dips are consistent with the phase boundaries obtained in Fig. 3(b).

To gain more insight into the vortex phases, we present the wave functions for phases V_I and V_{II} in Fig. 4. As shown in the phase plots, the spin-↑ state in phase V_I contains two singly quantized vortices and the spin-↓ state in phase V_{II} has a DQV, in striking difference to the vortices in dipolar spin-1 atomic condensates [29]. The presence of the vortices can be understood from $\hat{V}_3$ in the DDI. By annihilating a spin-↑ molecule and creating a spin-↓ molecule, the rotational angular momentum is decreased by $2\hbar$. To ensure the total angular momentum conservation, the orbital angular momentum of spin-↑ molecules must be larger than that of spin-↓ molecules by $2\hbar$, which gives rise to the vortex phases. However, for reasons which shall become clear below, the DQV in the spin-↑ state of phase V_I splits into two singly quantized states such that $|L_\uparrow^{(z)}|$ is smaller than $2\hbar$.

As to the density profiles, the spin-↑ molecules always occupy the center of the trap, with spin-↓ molecules being pushed to the periphery. This observation holds even if the scattering lengths are slightly tuned such that the contact

interactions favor a miscible gas. In fact, by aggregating at the trap center, the spin-↑ cloud becomes less oblate such that the intraspecies DDI, $\hat{V}_1$, is lowered. Additionally, in a less oblate dipolar condensate, a DQV becomes more unstable against splitting [43]. The immiscibility of the spin-↑ and -↓ clouds is induced by $\hat{V}_2$, as a miscible mixture in a pancake-shaped trap normally results in a positive dipolar spin-exchange interaction energy due to the anisotropic nature of Y_{20}. In this density configuration, spin-↑ gas acts effectively as a pinning potential for spin-↓ molecules, which stabilizes the DQV in spin-↓ state [44]. Nevertheless, this DQV can still split. In fact, in the vicinity of the stability boundary, the orbital angular momentum $L_{\downarrow}^{(z)}$ drops slightly, signaling the splitting of the DQV in the spin-↓ state.

This layered density structure also leads to other nontrivial behavior of the condensate. In dipolar spinor condensates, it is usually energetically favorable to have vortices emerge in the less populated spin state due to the kinetic energy associated with the vortex state. Here we see that near the phase boundary between $\mathrm{V_I}$ and $\mathrm{V_{II}}$, the vortex emerges in the spin-↓ state, even though $\mathcal{N}_{\downarrow}$ is still larger than $\mathcal{N}_{\uparrow}$. This can be understood as follows. Since the spin-↓ cloud occupies the outer layer, adding vortices to it will hardly modify its density profile and costs only the kinetic energy associated with the gradient of the phase. However, for the spin-↑ state, the appearance of vortices will significantly change its density profile, which results in extra kinetic energy contributed by the gradient of density. In fact, we have examined the kinetic energies contributed from each spin state in the vicinity of the phase boundary. It is found that the kinetic energy of the spin-↑ state drops dramatically during the transition from the $\mathrm{V_I}$ to $\mathrm{V_{II}}$ phases, while only a moderate change occurs for the kinetic energy of the spin-↓ state.

In Fig. 5(a), we plot the DDI energies as functions of κ. The negativity of $\langle\hat{V}_1\rangle$ indicates that the spin-↑ condensate is indeed of cigar shape, whereas it is confined is a pancake-shaped trap. Moreover, the fact that $\langle\hat{V}_2\rangle$ roughly remains zero over a wide range of κ is consistent with the immiscibility of the system. For $\langle\hat{V}_3\rangle$ it can be rewritten as

$$\langle\hat{V}_3\rangle = \kappa g_d \int \frac{d\mathbf{r}_1 d\mathbf{r}_2}{R^3} n_{\uparrow}(\mathbf{r}_1)\sin^2\theta_{\mathbf{R}} \times [s_x(\mathbf{r}_2)\cos(2\varphi_{\mathbf{R}}) + s_y(\mathbf{r}_2)\sin(2\varphi_{\mathbf{R}})], \quad (6)$$

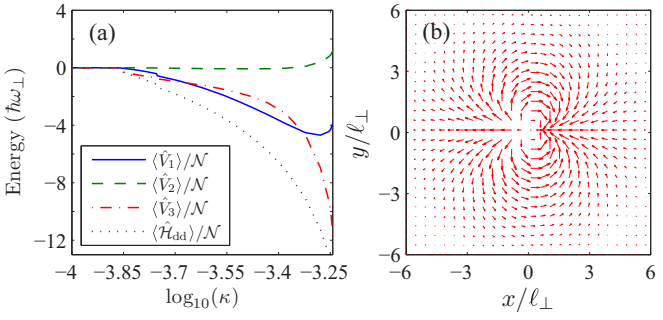

FIG. 5. (Color online) (a) κ dependence of the DDI energies per molecule for $\delta = 2\omega_\perp$. (b) Typical planar spin structure for the vortex phases.

where $\theta_{\mathbf{R}}$ and $\varphi_{\mathbf{R}}$ are the polar and azimuthal angles of $\mathbf{R}$, respectively, $s_x = \frac{1}{2}(\langle\hat{S}_+\rangle + \langle\hat{S}_-\rangle)$, and $s_y = \frac{1}{2i}(\langle\hat{S}_+\rangle - \langle\hat{S}_-\rangle)$. Clearly, $\hat{V}_3$ aligns the planar spin $\mathbf{s}_\perp = (s_x, s_y)$ such that $\langle\hat{V}_3\rangle$ is always negative. In fact, as shown in Fig. 5(b), $\mathbf{s}_\perp$ always forms a spin vortex with winding number 2 in the vortex phases. In competing with $\hat{V}_2$, it is energetically favorable to have a large overlap between $\psi_\uparrow$ and $\psi_\downarrow$ for $\hat{V}_3$. Consequently, $\langle\hat{V}_1\rangle$ and $\langle\hat{V}_2\rangle$ significantly increase with κ in the strong DDI regime. Since $\langle\hat{V}_3\rangle$ also depends on $n_\uparrow$, it explains why $\mathcal{N}_\uparrow$ continuously grows with κ [Fig. 2(b)], instead of being saturated at around $\mathcal{N}/2$. Finally, it is worthwhile to point out that the condensate becomes unstable when the DDI interaction energy is comparable to the contact interaction energy. The critical value of κ is insensitive to δ, as the spins are free to rearrange themselves to minimize the dipolar interaction energy.

V. EXPERIMENTAL FEASIBILITY

The realization of the proposed model requires the molecules to possess a large hyperfine splitting such that the effective DDI would not mix the unwanted rotational sublevel. In fact, the nuclear electric quadrupole coupling constants for all bialkali polar molecules with known molecular parameters are of order 100 kHz [36], indicating that the proposed scheme is also applicable to other bialkali polar molecules.

As to the experimental detection, similar to imaging an atomic spinor condensate, we may construct a Stern-Gerlach apparatus by utilizing the rotational Zeeman shift, $-g_r\mu_N\mathbf{N}\cdot\mathbf{B}$, where g_r is the rotational g factor of the molecule and μ_N is the nuclear magnetic moment. It can be estimated that for a modest magnetic field gradient of a few T/m, the spin-↑ and -↓ states of the LiCs molecules are spatially separated after 200 ms of free expansion and can be directly observed with absorption image measurement [45].

VI. CONCLUSIONS

We have demonstrated that a rotating bialkali polar molecule can be modeled as a pseudospin-1/2 particle by utilizing external magnetic and microwave fields. In this model, a control knob for the effective molecular DDI is naturally introduced that can be used to stabilize the condensates of polar molecules with large electric dipole moment. We have also shown that the rotation-orbit coupling term in the effective DDI gives rise to DQV phases of the molecular condensate. Finally, the proposed scheme also works for the ultracold gases of fermionic polar molecules, in which the effective DDI may lead to exotic superfluid pairings.

Note added. Recently, we became aware of the work by Wall *et al.* [46] for realizing unconventional quantum magnetism with symmetric top molecules in which the effective DDI also exchanges the spin and orbital angular momentum.

ACKNOWLEDGMENTS

This work was supported by the National 973 program (Grant No. 2012CB922104) and the NSFC (Grants No. 11434011, No. 11421063, and No. 11025421).

APPENDIX A: HYPERFINE STRUCTURE OF $^1\Sigma$ BIALKALI MOLECULES

Here we demonstrate how to reduce the internal states of a $^1\Sigma$ bialkali molecule to a four-level system. The Hamiltonian describing the internal degrees of freedom of a $^1\Sigma$ diatomic molecule subjected to a bias magnetic field $\mathbf{B} = B\hat{\mathbf{z}}$ is [36,38,47]

$$\hat{H}_{\rm in} = \hat{H}_{\rm rot} + \hat{H}_{\rm hf} + \hat{H}_Z, \tag{A1}$$

where $\hat{H}_{\rm rot} = B_v \mathbf{N}^2$ is diagonal in the uncoupled basis $\{|M_1 M_2 N M_N\rangle\}$.

The nuclear hyperfine interaction contains four contributions: nuclear electric quadrupole interaction $\hat{H}_Q$, nuclear spin-rotation interaction $\hat{H}_{IN}$, and tensor $\hat{H}_t$ and scalar $\hat{H}_{\rm sc}$ nuclear spin-spin interactions. Explicitly, the hyperfine Hamiltonian can be expressed as

$$\begin{aligned}\hat{H}_{\rm hf} =& \hat{H}_Q + \hat{H}_{IN} + \hat{H}_t + \hat{H}_{\rm sc} \\ =& \sum_{i=1}^{2} \frac{\sqrt{6}(eQ_i q_i)}{4I_i(2I_i-1)} T^{(2)}(\mathbf{C}) \cdot T^{(2)}(\mathbf{I}_i,\mathbf{I}_i) + \sum_{i=1}^{2} c_i \mathbf{N}\cdot\mathbf{I}_i - c_3\sqrt{6}\, T^{(2)}(\mathbf{C}) \cdot T^{(2)}(\mathbf{I}_1,\mathbf{I}_2) + c_4 \mathbf{I}_1\cdot\mathbf{I}_2,\end{aligned} \tag{A2}$$

where $T^{(2)}(\mathbf{C})$ is the second-order un-normalized spherical harmonic with components $T^{(2)}_q(\mathbf{C}) \equiv C^{(2)}_q(\theta,\varphi) = \sqrt{\frac{4\pi}{5}} Y_{2,q}(\theta,\varphi)$, with (θ,φ) being the spherical coordinate and $T^{(2)}(\mathbf{I}_i,\mathbf{I}_j)$ represents the spherical tensor operator of rank 2, formed by the vector operators $\mathbf{I}_i$ and $\mathbf{I}_j$. Moreover, eQ_i is the electric quadrupole moment of nucleus i, q_i characterizes the negative of the electric field gradient at nucleus i, c_i represents the strength of the nuclear spin-rotation coupling for the ith nucleus, and c_3 and c_4 are, respectively, the strengths of the nuclear tensor and scalar spin-spin interaction. The matrix elements of the hyperfine interaction in the uncoupled basis are [21,23,38]

$$\begin{aligned}\langle M_1 M_2 N M_N|\hat{H}_Q|M_1' M_2' N' M_N'\rangle =& \sum_{i=1,2} \frac{(eQq)_i}{4} \delta_{M_{\bar{i}} M_{\bar{i}}'} \sum_p (-1)^{p-M_N+I_i-M_i} \sqrt{(2N+1)(2N'+1)} \\ &\times \begin{pmatrix} N & 2 & N' \\ -M_N & p & M_N' \end{pmatrix} \begin{pmatrix} I_i & 2 & I_i \\ -M_i & -p & M_i' \end{pmatrix} \begin{pmatrix} N & 2 & N' \\ 0 & 0 & 0 \end{pmatrix} \begin{pmatrix} I_i & 2 & I_i \\ -I_i & 0 & I_i \end{pmatrix}^{-1},\end{aligned} \tag{A3}$$

$$\begin{aligned}\langle M_1 M_2 N M_N|\hat{H}_{IN}|M_1' M_2' N' M_N'\rangle =& \delta_{NN'} \sum_q (-1)^{q+N-M_N} \sqrt{N(N+1)(2N+1)} \begin{pmatrix} N & 1 & N \\ -M_N & q & M_N' \end{pmatrix} \\ &\times \sum_{i=1,2} c_i (-1)^{I_i-M_i} \delta_{M_{\bar{i}} M_{\bar{i}}'} \sqrt{I_i(I_i+1)(2I_i+1)} \begin{pmatrix} I_i & 1 & I_i \\ -M_i & -q & M_i' \end{pmatrix},\end{aligned} \tag{A4}$$

$$\begin{aligned}\langle M_1 M_2 N M_N|\hat{H}_t|M_1' M_2' N' M_N'\rangle =& -c_3\sqrt{6}\sqrt{I_1(I_1+1)(2I_1+1)}\sqrt{I_2(I_2+1)(2I_2+1)}\sqrt{(2N+1)(2N'+1)} \\ &\times \begin{pmatrix} N & 2 & N' \\ 0 & 0 & 0 \end{pmatrix} \sum_p (-1)^{p-M_N+I_1-M_1+I_2-M_2} \begin{pmatrix} N & 2 & N' \\ -M_N & p & M_N' \end{pmatrix} \\ &\times \sum_m \langle 1,m;1,-p-m|2,-p\rangle \begin{pmatrix} I_1 & 1 & I_1 \\ -M_1 & m & M_1' \end{pmatrix} \begin{pmatrix} I_2 & 1 & I_2 \\ -M_2 & -p-m & M_2' \end{pmatrix},\end{aligned} \tag{A5}$$

$$\begin{aligned}\langle M_1 M_2 N M_N|\hat{H}_{\rm sc}|M_1' M_2' N' M_N'\rangle =& c_4 \delta_{NN'} \delta_{M_N M_N'} \sqrt{I_1(I_1+1)(2I_1+1)}\sqrt{I_2(I_2+1)(2I_2+1)} \\ &\times (-1)^{I_1-M_1+I_2-M_2} \sum_p (-1)^p \begin{pmatrix} I_1 & 1 & I_2 \\ -M_1 & p & M_1' \end{pmatrix} \begin{pmatrix} I_2 & 1 & I_2 \\ -M_2 & -p & M_2' \end{pmatrix},\end{aligned} \tag{A6}$$

where $\bar{i} = 3 - i$.

Finally, the Hamiltonian describes the Zeeman term is

$$\hat{H}_Z = -g_r \mu_N \mathbf{N}\cdot\mathbf{B} - \sum_{i=1}^{2} g_i \mu_N \mathbf{I}_i \cdot \mathbf{B}(1-\sigma_i), \tag{A7}$$

where μ_N is the nuclear magnetic moment, g_r is the rotational g factor of the molecule, g_i is the nuclear g factor for the ith nucleus, and σ_i is the nuclear shielding parameter. Clearly, $\hat{H}_Z$ is diagonal in the uncoupled basis.

For convenience, we list in Table I, the molecular parameters for several bialkali molecules. As can be seen, the rotational constants are of order 1 GHz and therefore define the largest energy scale of the internal states. In addition, with the help of Eqs. (A3)–(A6), we note that (i) $\hat{H}_{IN}$ does not couple states with different N and it plays a very small role in the spectra due to the smallness of the parameters c_1 and c_2; (ii) $\hat{H}_t$ often has a negligible effect as c_3 is usually of order 10–100 Hz; (iii) $\hat{H}_Q$ does not affect the $N = 0$ level, however, it dominates for the $N = 1$ level; and (iv) $\hat{H}_{\rm sc}$ splits the various levels according to their total

TABLE I. Molecular parameters for bialkali polar molecules. Subscripts 1 and 2 refer to the less electronegative and to the more electronegative atom [20,36,39].

Molecule	^{7}Li ^{133}Cs	^{40}K ^{87}Rb	^{41}K ^{87}Rb	^{87}Rb ^{133}Cs
I_1	3/2	4	3/2	3/2
I_2	7/2	3/2	5/2	7/2
g_1	2.171	−0.324	0.143	1.834
g_2	0.738	1.834	0.541	0.738
B_v (GHz)	5.636	1.114	1.104	0.504
$(eqQ)_1$ (kHz)	18.5	452	−298	−872
$(eqQ)_2$ (kHz)	188	−1308	−1520	51
σ_1 (ppm)	108.2	1321	1321	3531
σ_2 (ppm)	6242.5	3469	3469	6367
c_1 (Hz)	32	−24.1	10.4	98.4
c_2 (Hz)	3014	420.1	413.1	194.1
c_3 (Hz)	140	−48.2	21.3	192.4
c_4 (Hz)	1610	−2030.4	896.2	17345.4
g_r	0.0106	0.0140	0.0138	0.0062
d (Debye)	5.52	0.566	0.566	1.25

nuclear spin I, and it is the dominant hyperfine contribution for $N = 0$ in the absence of external electric field.

To obtain the level structure shown in Fig. 1, we diagonalize $\hat{H}_{\rm in}$ in the uncoupled basis. The resulting eigenstates clearly show that M_1 and M_2 are good quantum numbers when B is larger than 40 G. Now we may focus on states with the same nuclear magnetic quantum numbers M_1 and M_2. Using Eqs. (A3)–(A6), it can be verified that the hyperfine interaction is diagonal in Hilbert space formed by four rotational levels in the $N = 0$ and 1 manifolds with given M_i. A convenient choice of the nuclear magnetic quantum numbers is to let $M_i = I_i$, which corresponds to the lowest nuclear Zeeman levels of the LiCs molecule. Within this Hilbert space, the effective Hamiltonian describing the internal degrees of the molecule now becomes

$$\hat{H}_{\rm in} = 2B_v \sum_{q=0,\pm1} |1,q\rangle\langle 1,q| + \hbar\delta_{1,-1}|1,1\rangle\langle 1,1| + \hbar\delta_{0,-1}|1,0\rangle\langle 1,0|. \tag{A8}$$

APPENDIX B: DERIVATION OF THE PSEUDOSPIN-1/2 SINGLE-PARTICLE HAMILTONIAN

Here we show that by applying a σ^+-polarized microwave field,

$$\mathbf{E}(t) = E_{\rm mw} e^{-i\omega_{\rm mw}t}\mathbf{e}_1 + \text{c.c.}, \tag{B1}$$

the reduced four-level system can be further simplified to a pseudospin-1/2 one, where $E_{\rm mw}$ is the position-independent amplitude and the spherical vectors $\hat{\mathbf{e}}_0 = \hat{\mathbf{z}}$ and $\hat{\mathbf{e}}_{\pm1} = \mp(\hat{\mathbf{x}} \pm i\hat{\mathbf{y}})/\sqrt{2}$ are defined in the space-fixed frame, representing the σ^+ ($\hat{\mathbf{e}}_1$), π ($\hat{\mathbf{e}}_0$), and σ^- ($\hat{\mathbf{e}}_{-1}$) polarization of the microwave with respect to the quantization z axis. The microwave field couples to the dipole moment $d\hat{\mathbf{d}}$ of the molecule through the Hamiltonian

$$\hat{H}_{\rm mw} = -d\hat{\mathbf{d}}\cdot\mathbf{E}(t) = -E_{\rm mw}(d_1 e^{-i\omega_{\rm mw}t} + d_1^\dagger e^{i\omega_{\rm mw}t}), \tag{B2}$$

where $d_q = d\hat{\mathbf{d}}\cdot\hat{\mathbf{e}}_q = dC_q^{(1)}(\theta,\varphi)$ with $C_q^{(1)}(\theta,\varphi) = \sqrt{\frac{4\pi}{3}}Y_{1,q}(\theta,\varphi)$. Now, the single-molecule Hamiltonian in the microwave field becomes

$$\hat{H}_{\rm in} + \hat{H}_{\rm mw} = 2B_v \sum_{q=0,\pm1} |1,q\rangle\langle 1,q| + \hbar\delta_{1,-1}|1,1\rangle\langle 1,1| + \hbar\delta_{0,-1}|1,0\rangle\langle 1,0| - \hbar\Omega(e^{-i\omega_{\rm mw}t}|1,1\rangle\langle 0,0| + \text{H.c.}), \tag{B3}$$

where the Rabi frequency is $\hbar\Omega = E_{\rm mw}\langle 1,1|d_1|0,0\rangle = dE_{\rm mw}/\sqrt{3}$.

To proceed further, we rewrite the Hamiltonian (B3) in terms of the annihilation operators $\hat{\psi}_{NM_N}$ as

$$\hat{H}_{\rm in} + \hat{H}_{\rm mw} = 2B_v \sum_{q=0,\pm1} \hat{\psi}_{1q}^\dagger\hat{\psi}_{1q} + \hbar\delta_{1,-1}\hat{\psi}_{11}^\dagger\hat{\psi}_{11} + \hbar\delta_{0,-1}\hat{\psi}_{10}^\dagger\hat{\psi}_{10} - \hbar\Omega(\hat{\psi}_{11}^\dagger\hat{\psi}_{00}e^{-i\omega_{\rm mw}t} + \text{H.c.}). \tag{B4}$$

We note that the spontaneous emissions of the excited rotational levels ($N = 1$) are ignored due to the long lifetime of the rotational state. By introducing a rotating frame defined by the unitary transformation

$$\mathcal{U} = \exp(-i\hat{H}'t/\hbar) \tag{B5}$$

with $\hat{H}' = \hbar\Delta\hat{\psi}_{00}^\dagger\hat{\psi}_{00} + 2B_v\sum_{q=0,\pm1}\hat{\psi}_{1q}^\dagger\hat{\psi}_{1q}$, we obtain the time-independent Hamiltonian

$$\begin{aligned}\hat{H}_{\rm in} + \hat{H}_{\rm mw} \to{}& \mathcal{U}^\dagger(\hat{H}_{\rm in} + \hat{H}_{\rm mw})\mathcal{U} - i\hbar\mathcal{U}^\dagger\frac{\partial}{\partial t}\mathcal{U},\\ ={}& \hbar[-\Delta\hat{\psi}_{00}^\dagger\hat{\psi}_{00} - \Omega(\hat{\psi}_{11}^\dagger\hat{\psi}_{00} + \text{H.c.})\\ &+ \delta_{1,-1}\hat{\psi}_{11}^\dagger\hat{\psi}_{11} + \delta_{0,-1}\hat{\psi}_{10}^\dagger\hat{\psi}_{10}].\end{aligned} \tag{B6}$$

In the rotating frame, the equations of motion for the annihilation operators are

$$\begin{aligned} i\dot{\hat{\psi}}_{00} &= -\Delta\hat{\psi}_{00} - \Omega\hat{\psi}_{11},\\ i\dot{\hat{\psi}}_{11} &= \delta_{1,-1}\hat{\psi}_{11} - \Omega\hat{\psi}_{00},\\ i\dot{\hat{\psi}}_{10} &= \delta_{0,-1}\hat{\psi}_{10},\\ i\dot{\hat{\psi}}_{1-1} &= 0.\end{aligned}$$

Assuming that all molecules are initially prepared in the $|1,1\rangle$ state and $|\Delta| \gg |\Omega|, |\delta_{1,-1}|, |\delta_{0,-1}|$, the $|0,0\rangle$ level can be adiabatically eliminated to yield

$$\hat{\psi}_{00} = -\frac{\Omega\hat{\psi}_{11}}{\Delta}. \tag{B7}$$

The adiabatic elimination of the $|0,0\rangle$ level also induces a Stark shift, Ω^2/Δ, to the $|1,1\rangle$ level, such that the effective single-particle Hamiltonian becomes

$$\hat{H}_{\rm in} + \hat{H}_{\rm mw} = \hbar(\delta\hat{\psi}_{11}^\dagger\hat{\psi}_{11} + \delta_{0,-1}\hat{\psi}_{10}^\dagger\hat{\psi}_{10}), \tag{B8}$$

with $\delta = \delta_{1,-1} + \Omega^2/\Delta$. Choosing $\delta/2$ as the origin of the energies, the above Hamiltonian can be rewritten as

$$\hat{H}_{\rm in} + \hat{H}_{\rm mw} = \hbar\left[\frac{\delta}{2}\hat{\psi}_{11}^\dagger\hat{\psi}_{11} + \left(\delta_{0,-1} - \frac{\delta}{2}\right)\hat{\psi}_{10}^\dagger\hat{\psi}_{10} - \frac{\delta}{2}\hat{\psi}_{1-1}^\dagger\hat{\psi}_{1-1}\right].$$

As analyzed in the main text, by choosing an appropriate Stark shift or magnetic field strength, we may realize the condition $|\delta| \ll |\delta_{0,-1}|$. Consequently, the $|1,0\rangle$ states becomes well separated from the nearly degenerate $|1,\pm1\rangle$ states, even in the presence of the molecule-molecule interactions (see below). After dropping the $|1,0\rangle$ state and taking into account the center-of-mass motion, we finally obtain the effective spin-1/2 single-molecule Hamiltonian, Eq. (2).

APPENDIX C: DERIVATION OF THE DDI IN THE PSEUDOSPIN-1/2 SYSTEM

For convenience, let us first write down the matrix elements of the dipole moment operator $\mathbf{d}$ in the rotational state basis $|NM_N\rangle$:

$$\langle NM_N|d_q|N'M'_N\rangle = (-1)^{2N-M_N} d\sqrt{(2N+1)(2N'+1)} \begin{pmatrix} N & 1 & N' \\ -M_N & q & M'_N \end{pmatrix} \begin{pmatrix} N & 1 & N' \\ 0 & 0 & 0 \end{pmatrix}. \tag{C1}$$

In the Hilbert space $\{|0,0\rangle,|1,0\rangle,|1,\pm1\rangle\}$, the dipole-dipole interaction (DDI), in the second-quantized form, reads

$$\begin{aligned}
\hat{\mathcal{H}}_{\rm dd} = {} & \frac{g_d}{2}\sqrt{\frac{16\pi}{45}} \int \frac{d\mathbf{r}_1 d\mathbf{r}_2}{|\mathbf{R}|^3} \{Y_{20}(\hat{\mathbf{R}})[\hat{\psi}^\dagger_{00}(\mathbf{r}_1)\hat{\psi}^\dagger_{11}(\mathbf{r}_2)\hat{\psi}_{00}(\mathbf{r}_2)\hat{\psi}_{11}(\mathbf{r}_1) + \hat{\psi}^\dagger_{00}(\mathbf{r}_1)\hat{\psi}^\dagger_{1-1}(\mathbf{r}_2)\hat{\psi}_{00}(\mathbf{r}_2)\hat{\psi}_{1-1}(\mathbf{r}_1) \\
& - 2\hat{\psi}^\dagger_{00}(\mathbf{r}_1)\hat{\psi}^\dagger_{10}(\mathbf{r}_2)\hat{\psi}_{00}(\mathbf{r}_2)\hat{\psi}_{1,0}(\mathbf{r}_1)] - Y_{20}(\hat{\mathbf{R}})[\hat{\psi}^\dagger_{00}(\mathbf{r}_1)\hat{\psi}^\dagger_{00}(\mathbf{r}_2)\hat{\psi}_{1-1}(\mathbf{r}_2)\hat{\psi}_{11}(\mathbf{r}_1) + \hat{\psi}^\dagger_{00}(\mathbf{r}_1)\hat{\psi}^\dagger_{00}(\mathbf{r}_2)\hat{\psi}_{10}(\mathbf{r}_2)\hat{\psi}_{10}(\mathbf{r}_1) + \text{H.c.}]\} \\
& - \frac{g_d}{2}\sqrt{\frac{16\pi}{15}} \int \frac{d\mathbf{r}_1 d\mathbf{r}_2}{|\mathbf{R}|^3} \{Y_{2-1}(\hat{\mathbf{R}})[\hat{\psi}^\dagger_{00}(\mathbf{r}_1)\hat{\psi}^\dagger_{00}(\mathbf{r}_2)\hat{\psi}_{1-1}(\mathbf{r}_2)\hat{\psi}_{10}(\mathbf{r}_1) + \hat{\psi}^\dagger_{00}(\mathbf{r}_1)\hat{\psi}^\dagger_{10}(\mathbf{r}_2)\hat{\psi}_{00}(\mathbf{r}_2)\hat{\psi}_{1-1}(\mathbf{r}_1) \\
& - \hat{\psi}^\dagger_{00}(\mathbf{r}_1)\hat{\psi}^\dagger_{11}(\mathbf{r}_2)\hat{\psi}_{00}(\mathbf{r}_2)\hat{\psi}_{10}(\mathbf{r}_1) - \hat{\psi}^\dagger_{11}(\mathbf{r}_1)\hat{\psi}^\dagger_{10}(\mathbf{r}_2)\hat{\psi}_{00}(\mathbf{r}_2)\hat{\psi}_{00}(\mathbf{r}_1)] + \text{H.c.}\} \\
& - \frac{g_d}{2}\sqrt{\frac{8\pi}{15}} \int \frac{d\mathbf{r}_1 d\mathbf{r}_2}{|\mathbf{R}|^3} \{Y_{2-2}(\hat{\mathbf{R}})[\hat{\psi}^\dagger_{00}(\mathbf{r}_1)\hat{\psi}^\dagger_{00}(\mathbf{r}_2)\hat{\psi}_{1,-1}(\mathbf{r}_2)\hat{\psi}_{1,-1}(\mathbf{r}_1) - 2\hat{\psi}^\dagger_{11}(\mathbf{r}_1)\hat{\psi}^\dagger_{00}(\mathbf{r}_2)\hat{\psi}_{1-1}(\mathbf{r}_2)\hat{\psi}_{00}(\mathbf{r}_1) \\
& + \hat{\psi}^\dagger_{11}(\mathbf{r}_1)\hat{\psi}^\dagger_{11}(\mathbf{r}_2)\hat{\psi}_{00}(\mathbf{r}_2)\hat{\psi}_{00}(\mathbf{r}_1)] + \text{H.c.}\},
\end{aligned} \tag{C2}$$

where we have arranged all terms according to the components of the spherical harmonics. From Eq. (C2), it is apparent that the DDI conserves the total (rotational + orbital) angular momentum. Next, in the presence of the microwave field, we apply the same unitary transformation, Eq. (B5), which yields the DDI Hamiltonian in the rotating frame as

$$\begin{aligned}
\hat{\mathcal{H}}_{\rm dd} \to \mathcal{U}^\dagger \hat{\mathcal{H}}_{\rm dd} \mathcal{U} = {} & \frac{g_d}{2}\sqrt{\frac{16\pi}{45}} \int \frac{d\mathbf{r}_1 d\mathbf{r}_2}{|\mathbf{R}|^3} \{Y_{20}(\hat{\mathbf{R}})[\hat{\psi}^\dagger_{00}(\mathbf{r}_1)\hat{\psi}^\dagger_{11}(\mathbf{r}_2)\hat{\psi}_{00}(\mathbf{r}_2)\hat{\psi}_{11}(\mathbf{r}_1) + \hat{\psi}^\dagger_{00}(\mathbf{r}_1)\hat{\psi}^\dagger_{1-1}(\mathbf{r}_2)\hat{\psi}_{00}(\mathbf{r}_2)\hat{\psi}_{1-1}(\mathbf{r}_1) \\
& - 2\hat{\psi}^\dagger_{00}(\mathbf{r}_1)\hat{\psi}^\dagger_{1,0}(\mathbf{r}_2)\hat{\psi}_{00}(\mathbf{r}_2)\hat{\psi}_{10}(\mathbf{r}_1)] - Y_{20}(\hat{\mathbf{R}})[\hat{\psi}^\dagger_{00}(\mathbf{r}_1)\hat{\psi}^\dagger_{00}(\mathbf{r}_2)\hat{\psi}_{1-1}(\mathbf{r}_2)\hat{\psi}_{11}(\mathbf{r}_1)e^{-2i\omega_{\rm mw}t} \\
& + \hat{\psi}^\dagger_{00}(\mathbf{r}_1)\hat{\psi}^\dagger_{00}(\mathbf{r}_2)\hat{\psi}_{10}(\mathbf{r}_2)\hat{\psi}_{10}(\mathbf{r}_1)e^{-2i\omega_{\rm mw}t} + \text{H.c.}]\} \\
& - \frac{g_d}{2}\sqrt{\frac{16\pi}{15}} \int \frac{d\mathbf{r}_1 d\mathbf{r}_2}{|\mathbf{R}|^3} \{Y_{2-1}(\hat{\mathbf{R}})[\hat{\psi}^\dagger_{00}(\mathbf{r}_1)\hat{\psi}^\dagger_{00}(\mathbf{r}_2)\hat{\psi}_{1-1}(\mathbf{r}_2)\hat{\psi}_{10}(\mathbf{r}_1)e^{-2i\omega_{\rm mw}t} + \hat{\psi}^\dagger_{00}(\mathbf{r}_1)\hat{\psi}^\dagger_{10}(\mathbf{r}_2)\hat{\psi}_{00}(\mathbf{r}_2)\hat{\psi}_{1-1}(\mathbf{r}_1) \\
& - \hat{\psi}^\dagger_{00}(\mathbf{r}_1)\hat{\psi}^\dagger_{11}(\mathbf{r}_2)\hat{\psi}_{00}(\mathbf{r}_2)\hat{\psi}_{10}(\mathbf{r}_1) - \hat{\psi}^\dagger_{11}(\mathbf{r}_1)\hat{\psi}^\dagger_{10}(\mathbf{r}_2)\hat{\psi}_{00}(\mathbf{r}_2)\hat{\psi}_{00}(\mathbf{r}_1)e^{2i\omega_{\rm mw}t}] + \text{H.c.}\} \\
& - \frac{g_d}{2}\sqrt{\frac{8\pi}{15}} \int \frac{d\mathbf{r}_1 d\mathbf{r}_2}{|\mathbf{R}|^3} \{Y_{2-2}(\hat{\mathbf{R}})[\hat{\psi}^\dagger_{00}(\mathbf{r}_1)\hat{\psi}^\dagger_{00}(\mathbf{r}_2)\hat{\psi}_{1-1}(\mathbf{r}_2)\hat{\psi}_{1-1}(\mathbf{r}_1)e^{-2i\omega_{\rm mw}t} - 2\hat{\psi}^\dagger_{11}(\mathbf{r}_1)\hat{\psi}^\dagger_{00}(\mathbf{r}_2)\hat{\psi}_{1-1}(\mathbf{r}_2)\hat{\psi}_{00}(\mathbf{r}_1) \\
& + \hat{\psi}^\dagger_{11}(\mathbf{r}_1)\hat{\psi}^\dagger_{11}(\mathbf{r}_2)\hat{\psi}_{00}(\mathbf{r}_2)\hat{\psi}_{00}(\mathbf{r}_1)e^{2i\omega_{\rm mw}t}] + \text{H.c.}\}.
\end{aligned} \tag{C3}$$

As estimated in the main text, the rotational splitting $2B_v$ is much larger than the DDI energy for a typical gas density. Consequently, the spin dynamics induced by the DDI is much slower than the Rabi oscillations induced by the microwave field. We may therefore use an effective DDI which is time-averaged over a period of $2\pi/\omega_{\rm mw}$, i.e.,

$$\begin{aligned}
\hat{\mathcal{H}}_{\rm dd} \simeq {} & \frac{g_d}{2}\sqrt{\frac{16\pi}{45}} \int \frac{d\mathbf{r}_1 d\mathbf{r}_2}{|\mathbf{R}|^3} \{Y_{20}(\hat{\mathbf{R}})[\hat{\psi}^\dagger_{00}(\mathbf{r}_1)\hat{\psi}^\dagger_{11}(\mathbf{r}_2)\hat{\psi}_{00}(\mathbf{r}_2)\hat{\psi}_{11}(\mathbf{r}_1) + \hat{\psi}^\dagger_{00}(\mathbf{r}_1)\hat{\psi}^\dagger_{1-1}(\mathbf{r}_2)\hat{\psi}_{00}(\mathbf{r}_2)\hat{\psi}_{1-1}(\mathbf{r}_1) \\
& - 2\hat{\psi}^\dagger_{00}(\mathbf{r}_1)\hat{\psi}^\dagger_{1,0}(\mathbf{r}_2)\hat{\psi}_{00}(\mathbf{r}_2)\hat{\psi}_{10}(\mathbf{r}_1)]\} - \frac{g_d}{2}\sqrt{\frac{16\pi}{15}} \int \frac{d\mathbf{r}_1 d\mathbf{r}_2}{|\mathbf{R}|^3} \{Y_{2-1}(\hat{\mathbf{R}})[\hat{\psi}^\dagger_{00}(\mathbf{r}_1)\hat{\psi}^\dagger_{10}(\mathbf{r}_2)\hat{\psi}_{00}(\mathbf{r}_2)\hat{\psi}_{1-1}(\mathbf{r}_1) \\
& - \hat{\psi}^\dagger_{00}(\mathbf{r}_1)\hat{\psi}^\dagger_{11}(\mathbf{r}_2)\hat{\psi}_{00}(\mathbf{r}_2)\hat{\psi}_{10}(\mathbf{r}_1)] + \text{H.c.}\} - \frac{g_d}{2}\sqrt{\frac{8\pi}{15}} \int \frac{d\mathbf{r}_1 d\mathbf{r}_2}{|\mathbf{R}|^3} [-2Y_{2-2}(\hat{\mathbf{R}})\hat{\psi}^\dagger_{11}(\mathbf{r}_1)\hat{\psi}^\dagger_{00}(\mathbf{r}_2)\hat{\psi}_{1-1}(\mathbf{r}_2)\hat{\psi}_{00}(\mathbf{r}_1) + \text{H.c.}].
\end{aligned} \tag{C4}$$

The adiabatic elimination of the $|0,0\rangle$ level from the interaction Hamiltonian (C4) can be achieved by simply performing the substitution $\hat{\psi}_{00} = -\Omega\hat{\psi}_{11}/\Delta$, which leads to

$$\begin{aligned}\hat{\mathcal{H}}_{\rm dd} \simeq & \frac{\kappa g_d}{2}\sqrt{\frac{16\pi}{45}}\int\frac{d\mathbf{r}_1 d\mathbf{r}_2}{|\mathbf{R}|^3}\{Y_{20}(\hat{\mathbf{R}})[\hat{\psi}_{11}^\dagger(\mathbf{r}_1)\hat{\psi}_{11}^\dagger(\mathbf{r}_2)\hat{\psi}_{11}(\mathbf{r}_2)\hat{\psi}_{11}(\mathbf{r}_1) + \hat{\psi}_{11}^\dagger(\mathbf{r}_1)\hat{\psi}_{1-1}^\dagger(\mathbf{r}_2)\hat{\psi}_{11}(\mathbf{r}_2)\hat{\psi}_{1-1}(\mathbf{r}_1) \\ & - 2\hat{\psi}_{11}^\dagger(\mathbf{r}_1)\hat{\psi}_{1,0}^\dagger(\mathbf{r}_2)\hat{\psi}_{11}(\mathbf{r}_2)\hat{\psi}_{10}(\mathbf{r}_1)]\} - \frac{\kappa g_d}{2}\sqrt{\frac{16\pi}{15}}\int\frac{d\mathbf{r}_1 d\mathbf{r}_2}{|\mathbf{R}|^3}\{Y_{2-1}(\hat{\mathbf{R}})[\hat{\psi}_{11}^\dagger(\mathbf{r}_1)\hat{\psi}_{10}^\dagger(\mathbf{r}_2)\hat{\psi}_{11}(\mathbf{r}_2)\hat{\psi}_{1-1}(\mathbf{r}_1) \\ & - \hat{\psi}_{11}^\dagger(\mathbf{r}_1)\hat{\psi}_{11}^\dagger(\mathbf{r}_2)\hat{\psi}_{11}(\mathbf{r}_2)\hat{\psi}_{10}(\mathbf{r}_1)] + \text{H.c.}\} - \frac{\kappa g_d}{2}\sqrt{\frac{8\pi}{15}}\int\frac{d\mathbf{r}_1 d\mathbf{r}_2}{|\mathbf{R}|^3}[-2Y_{2-2}(\hat{\mathbf{R}})\hat{\psi}_{11}^\dagger(\mathbf{r}_1)\hat{\psi}_{11}^\dagger(\mathbf{r}_2)\hat{\psi}_{1-1}(\mathbf{r}_2)\hat{\psi}_{11}(\mathbf{r}_1) + \text{H.c.}].\end{aligned} \tag{C5}$$

As can be seen, the elimination of $|0,0\rangle$ level gives rise to the factor κ to the DDI strength, which can be used as a control knob for the DDI. For the parameter regime considered in this work, the DDI energy $\kappa g_d n$ is much smaller than the level splitting between $|1,0\rangle$ and $|1,\pm1\rangle$. Therefore, with the assumption that all molecules are prepared in the $|1,1\rangle$ state, the $|1,0\rangle$ level is essentially unoccupied during the time scale considered here. As a result, we may simply drop all terms containing $\hat{\psi}_{10}$ in $\hat{\mathcal{H}}_{\rm dd}$, which eventually leads to the effective DDI Hamiltonian, Eq. (4).

[1] K.-K. Ni, S. Ospelkaus, M. H. G. de Miranda, A. Péer, B. Neyenhuis, J. J. Zirbel, S. Kotochigova, P. S. Julienne, D. S. Jin, and J. Ye, Science **322**, 231 (2008).

[2] J. Deiglmayr, A. Grochola, M. Repp, K. Mörtlbauer, C. Glück, J. Lange, O. Dulieu, R. Wester, and M. Weidemüller, Phys. Rev. Lett. **101**, 133004 (2008).

[3] T. Takekoshi, L. Reichsöllner, A. Schindewolf, J. M. Hutson, C. R. Le Sueur, O. Dulieu, F. Ferlaino, R. Grimm, and H.-C. Nägerl, Phys. Rev. Lett. **113**, 205301 (2014).

[4] T. Shimasaki, M. Bellos, C. D. Bruzewicz, Z. Lasner, and D. DeMille, Phys. Rev. A **91**, 021401(R) (2015).

[5] P. K. Molony, P. D. Gregory, Z. Ji, B. Lu, M. P. Köppinger, C. R. Le Sueur, C. L. Blackley, J. M. Hutson, and S. L. Cornish, Phys. Rev. Lett. **113**, 255301 (2014).

[6] J. W. Park, S. A. Will, and M. W. Zwierlein, Phys. Rev. Lett. **114**, 205302 (2015).

[7] V. V. Flambaum and M. G. Kozlov, Phys. Rev. Lett. **99**, 150801 (2007).

[8] T. A. Isaev, S. Hoekstra, and R. Berger, Phys. Rev. A **82**, 052521 (2010).

[9] J. J. Hudson, D. M. Kara, I. J. Smallman, B. E. Sauer, M. R. Tarbutt, and E. A. Hinds, Nature (London) **473**, 493 (2011).

[10] P. Rabl, D. DeMille, J. M. Doyle, M. D. Lukin, R. J. Schoelkopf, and P. Zoller, Phys. Rev. Lett. **97**, 033003 (2006).

[11] D. DeMille, Phys. Rev. Lett. **88**, 067901 (2002).

[12] K.-K. Ni, S. Ospelkaus, D. Wang, G. Quéméner, B. Neyenhuis, M. H. G. de Miranda, J. L. Bohn, J. Ye, and D. S. Jin, Nature (London) **464**, 1324 (2010).

[13] J. Deiglmayr, M. Repp, R. Wester, O. Dulieud, and M. Weidemüller, Phys. Chem. Chem. Phys. **13**, 19101 (2011).

[14] S. Ospelkaus, K.-K. Ni, D. Wang, M. H. G. de Miranda, B. Neyenhuis, G. Quéméner, P. S. Julienne, J. L. Bohn, D. S. Jin, and J. Ye, Science **327**, 853 (2010).

[15] M. H. G. de Miranda, A. Chotia1, B. Neyenhuis, D. Wang, G. Quéméner, S. Ospelkaus, J. L. Bohn, J. Ye, and D. S. Jin, Nat. Phys. **7**, 502 (2011).

[16] A. Micheli, G. K. Brennen, and P. Zoller, Nat. Phys. **2**, 341 (2006).

[17] R. Barnett, D. Petrov, M. Lukin, and E. Demler, Phys. Rev. Lett. **96**, 190401 (2006).

[18] M. A. Baranov, M. Dalmonte, G. Pupillo, and P. Zoller, Chem. Rev. **112**, 5012 (2012).

[19] S. Ospelkaus, K.-K. Ni, G. Quéméner, B. Neyenhuis, D. Wang, M. H. G. de Miranda, J. L. Bohn, J. Ye, and D. S. Jin, Phys. Rev. Lett. **104**, 030402 (2010).

[20] B. Neyenhuis, B. Yan, S. A. Moses, J. P. Covey, A. Chotia, A. Petrov, S. Kotochigova, J. Ye, and D. S. Jin, Phys. Rev. Lett. **109**, 230403 (2012).

[21] M. L. Wall and L. D. Carr, Phys. Rev. A **82**, 013611 (2010).

[22] A. V. Gorshkov, S. R. Manmana, G. Chen, J. Ye, E. Demler, M. D. Lukin, and A. M. Rey, Phys. Rev. Lett. **107**, 115301 (2011).

[23] A. V. Gorshkov, S. R. Manmana, G. Chen, E. Demler, M. D. Lukin, and A. M. Rey, Phys. Rev. A **84**, 033619 (2011).

[24] B. Yan, S. A. Moses, B. Gadway, J. P. Covey, K. R. A. Hazzard, A. M. Rey, D. S. Jin, and J. Ye, Nature (London) **501**, 512 (2013).

[25] K. R. A. Hazzard, B. Gadway, M. Foss-Feig, B. Yan, S. A. Moses, J. P. Covey, N. Y. Yao, M. D. Lukin, J. Ye, D. S. Jin, and A. M. Rey, Phys. Rev. Lett. **113**, 195302 (2014).

[26] T.-L. Ho, Phys. Rev. Lett. **81**, 742 (1998).

[27] T. Ohmi and K. Machida, J. Phys. Soc. Jpn. **67**, 1822 (1998).

[28] C. K. Law, H. Pu, and N. P. Bigelow, Phys. Rev. Lett. **81**, 5257 (1998).

[29] S. Yi and H. Pu, Phys. Rev. Lett. **97**, 020401 (2006).

[30] Y. Kawaguchi, H. Saito, and M. Ueda, Phys. Rev. Lett. **97**, 130404 (2006).

[31] M. Vengalattore, S. R. Leslie, J. Guzman, and D. M. Stamper-Kurn, Phys. Rev. Lett. **100**, 170403 (2008).

[32] Y. Eto, H. Saito, and T. Hirano, Phys. Rev. Lett. **112**, 185301 (2014).

[33] C.-H. Lin, Y.-T. Hsu, H. Lee, and D.-W. Wang, Phys. Rev. A **81**, 031601(R) (2010).

[34] J. Armaitis, R. A. Duine, and H. T. C. Stoof, Phys. Rev. Lett. **111**, 215301 (2013).

[35] R. M. Wilson, B. M. Peden, C. W. Clark, and S. T. Rittenhouse, Phys. Rev. Lett. **112**, 135301 (2014).

[36] J. Aldegunde, B. A. Rivington, P. S. Żuchowski, and J. M. Hutson, Phys. Rev. A **78**, 033434 (2008).

[37] J. Aldegunde, H. Ran, and J. M. Hutson, Phys. Rev. A **80**, 043410 (2009).

[38] J. Aldegunde and J. M. Hutson, Phys. Rev. A **79**, 013401 (2009).

[39] H. Ran, J. Aldegunde, and J. M. Hutson, New J. Phys. **12**, 043015 (2010).

[40] Although $\Delta\kappa$ is not a constant in Fig. 3(d) as limited by the available data points, $\Delta\kappa$ has the smallest values near the phase boundaries.

[41] H. T. Quan, Z. Song, X. F. Liu, P. Zanardi, and C. P. Sun, Phys. Rev. Lett. **96**, 140604 (2006).

[42] S. J. Gu, Int. J. Mod. Phys. B **24**, 4371 (2010).

[43] R. M. Wilson, S. Ronen, and J. L. Bohn, Phys. Rev. A **79**, 013621 (2009).

[44] T. P. Simula, S. M. M. Virtanen, and M. M. Salomaa, Phys. Rev. A **65**, 033614 (2002).

[45] D. Wang, B. Neyenhuis, M. H. G. de Miranda, K.-K. Ni, S. Ospelkaus, D. S. Jin, and J. Ye, Phys. Rev. A **81**, 061404(R) (2010).

[46] M. L. Wall, K. Maeda, and L. D. Carr, New J. Phys. **17**, 025001 (2015).

[47] J. M. Brown and A. Carrington, *Rotational Spectroscopy of Diatomic Molecules* (Cambridge University Press, Cambridge, UK, 2003).